The U^{5+} compound Ba_9Ag_10U_4S_24: Synthesis, structure, and electronic properties

Adel Mesbah, Wojciech Stojko, Sébastien Lebègue, Christos D. Malliakas, N. Laszlo Frazer, James A. Ibers

▶ **To cite this version:**

Adel Mesbah, Wojciech Stojko, Sébastien Lebègue, Christos D. Malliakas, N. Laszlo Frazer, et al.. The U^{5+} compound Ba_9Ag_10U_4S_24: Synthesis, structure, and electronic properties. Journal of Solid State Chemistry, 2015, 221, pp.398-404. 10.1016/j.jssc.2014.10.014 . hal-01521898

HAL Id: hal-01521898

https://hal.univ-lorraine.fr/hal-01521898

Submitted on 29 Apr 2019

HAL is a multi-disciplinary open access archive for the deposit and dissemination of scientific research documents, whether they are published or not. The documents may come from teaching and research institutions in France or abroad, or from public or private research centers.

L'archive ouverte pluridisciplinaire **HAL**, est destinée au dépôt et à la diffusion de documents scientifiques de niveau recherche, publiés ou non, émanant des établissements d'enseignement et de recherche français ou étrangers, des laboratoires publics ou privés.

The U^{5+} compound $Ba_9Ag_{10}U_4S_{24}$: synthesis, structure, and electronic properties

© 2014. This manuscript version is made available under the Elsevier user license
http://www.elsevier.com/open-access/userlicense/1.0/

Adel Mesbah,[a,b] Wojciech Stojko,[a] Sébastien Lebègue,[c] Christos D. Malliakas,[a] N. Laszlo Frazer,[d] and James A. Ibers[a,*]

[a]*Department of Chemistry, Northwestern University, 2145 Sheridan Road, Evanston, IL 60208-3113, United States*

[b] *ICSM, UMR 5257 CEA / CNRS / UM2 / ENSCM, Site de Marcoule - Bât. 426, BP 17171, 30207 Bagnols-sur-Cèze cedex, France*

[c]*Laboratoire de Cristallographie, Résonance Magnétique, et Modélisations CRM2 (UMR UHP-CNRS 7036), Faculté des Sciences et Techniques, Université de Lorraine, BP 70239, Boulevard des Aiguillettes, 54506 Vandoeuvre-lès-Nancy Cedex, France*

[d]*Department of Physics and Astronomy, Northwestern University, 2145 Sheridan Road, Evanston, IL 60208-3112, United States*

Keywords: synthesis; single-crystal X-ray structure; U^{5+}; resistivity; DFT calculations; spectroscopy.

ABSTRACT: Black crystals of $Ba_9Ag_{10}U_4S_{24}$ have been made by direct combination of BaS, Ag, U, and S at 1273 K. This compound crystallizes in a new structure type in the space group C_{4v}^{10}–$I4cm$ of the tetragonal system with four formula units in a cell with lattice constants a = 13.9189(6) Å and c = 23.7641(11) Å (V = 4604(5) Å^3). Multiphoton Luminescence Spectroscopy measurements are consistent with the noncentrosymmetric nature of the structure. In the structure each U atom is octahedrally coordinated by six S atoms, whereas three of the five crystallographically independent Ag atoms are tetrahedrally coordinated to four S atoms, another has a seesaw coordination to four S atoms, and the last has a triangular coordination to three S atoms. The overall structure consists of the three-dimensional stacking of the US_6, AgS_4, and AgS_3 polyhedra to leave channels in which Ba atoms reside. Based on the values of the U–S interatomic distances, the compound $Ba_9Ag_{10}U_4S_{24}$ contains U^{5+} and charge balance is achieved with the formal oxidation states of 9 Ba^{2+}, 10 Ag^{1+}, 4 U^{5+} and 24 S^{2-}. DFT calculations predict an antiferromagnetic ground state and a band gap of 2.1 eV. Resistivity measurements indicate that the compound is a semiconductor with a complex activation mechanism and activation energies ranging from 0.03(1) eV to 0.08(1) eV.

* Corresponding author: Fax: +1 847 491 2976

E-mail address: ibers@chem.northwestern.edu [J.A.Ibers]

1. Introduction

The chemistry of actinide-based compounds is but a niche in the vast chemistry of the elements. However, from a fundamental point of view it shows some unusual features and, of course, it is of practical importance in the nuclear fuel cycle as a source of sustainable energy. The 5f elements exhibit variable oxidation states whether in solution or in solid-state compounds. Uranium presents an excellent example with oxidation states varying between +3 and +6. The most stable are +4 and +6, and the stabilization of other oxidation states is often difficult. Because U^{5+} species easily disproportionate to U^{4+} and U^{6+} species, U^{5+} compounds are rare and most were synthesized serendipitously. Advances have been made concerning the controlled syntheses and the understanding of the physical properties of U^{5+} ($5f^1$) compounds, especially among molecular compounds [1], hydrated inorganic materials [2-4], and solid-state oxides [5,6]. However, this is not so for solid-state uranium chalcogenides (chalcogen = Q = S, Se, or Te) [7-9]. Many such compounds have been synthesized by the direct combination of elements or by the use of the reactive flux method [10]. The vast majority of these contain U^{4+}. However, a few contain U^{3+}, namely U_2S_3 [11], PdU_2S_4 [12], $ScUS_3$ [12], and ScU_3S_6 [13] and some contain U^{5+}, namely $Rb_4U_4P_4Se_{26}$ [14], $Tl_3Cu_4USe_6$ [15], $K_2Cu_3US_5$ [16], and Ba_3AgUS_6 [17]. Mixed oxidation states have also been reported, namely ScU_8S_{17} [18,19], $U_xPd_3S_4$ [20,21] (+3/+4), $Ba_{3.69}US_6$ [22] and $Ba_8Hg_3U_3S_{18}$ [23] (+4/+5), and $A_6Cu_{12}U_2S_{15}$ (A = K, Rb, Cs) (+5/+6) [24].

Because three of the above examples contain both Ba^{2+} and U^{5+}we continue here our exploration of such systems. Thus, in this paper we report the synthesis, structure, and characterization of the new quaternary barium uranium chalcogenide $Ba_9Ag_{10}U_4S_{24}$, which we show is a compound of U^{5+}.

2. Experimental

2.1. Synthesis

Depleted U turnings (Oak Ridge National Laboratory) were powdered by hydrization and the resultant hydride was decomposed by heating under vacuum in a modification [25] of a previous literature method [26]. The other reactants were used as supplied: BaS (Alfa, 99.7%), Ag (Aldrich, 99.99%), and S (Mallinckrodt, 99.6%).

Single crystals of what turned out to be $Ba_9Ag_{10}U_4S_{24}$ were obtained first in low yield (10%), when we attempted to synthesize the silver analogue of $Ba_2Cu_2AnS_5$ (An=Th,U) [27,28]. Subsequently, we found a high-yield route to $Ba_9Ag_{10}U_4S_{24}$ that involved direct combination of U (30 mg, 0.125 mmol), BaS (42.2 mg, 0.25 mmol), Ag (27.1 mg, 0.25 mmol), and S (20.2 mg, 0.63 mmol). The mixture was loaded into a carbon-coated fused-silica tube under an Ar atmosphere in a glovebox, transferred out of the box by the use of special adaptors to avoid oxygen contamination, then evacuated to 10^{-4} Torr, and flame sealed. The tube was placed in a computer-controlled furnace, heated to 1273 K in 48 h, kept there for 8 d, then cooled to 298 K at 3 Kh^{-1}. The resultant black blocks were obtained in about 90 wt% yield. EDX analysis of the crystals using an Hitachi 3400 SEM showed the presence of Ba:Ag:U:S≈2:2:1:6.

2.2. Structure determination

Single-crystal X-ray diffraction data were collected at 100(2) K on a Bruker APEX2 Kappa diffractometer equipped with graphite-monochromatized MoKα radiation (λ = 0.71073 Å). Data-collection strategy obtained by the algorithm COSMO in the APEX2 package comprised ω and ϕ scans [29]. The step size was 0.3 º and exposure time was 10 s/frame. Data were indexed, refined, and integrated with the program SAINT in the APEX2 package [29]. Numerical face-indexed absorption corrections were applied with the use of the program SADABS [30]. The precession images showed no evidence of a superstructure. However, merohedral twinning was detected through the use the TwinRotMat routine as implemented in

PLATON [31]. The crystal structure was solved and refined in the non-centrosymmetric space group C_{4v}^{10}–*I*4*cm* with the use of the Shelx-14 program package [30,32]. The refined twinning ratio is 0.512(9):0.488(9). All attempts to solve this structure in the centrosymmetric space group D_{4h}^{18}–*I*4/*mcm* failed. The program STRUCTURE TIDY [33] in PLATON [31] was used to standardize the atomic positions. Crystal structure data and the refinement parameters are given in Table 1 and in the Supporting Information.

2.3. Multiphoton luminescence spectroscopy

The 1064 nm beam of a Nd:YAG 32.5 ps pulsed laser producing 4.44(7) mJ per shot was focused to a spot size of about 1 mm diameter onto the sample (ground single crystals). The beam was filtered to remove any second harmonic generation that occurred in the laser. Luminescence from the sample was collected off the beam axis through a 930 nm short wavelength passing filter into a time averaging CCD spectrometer. Seventeen grating positions were used to collect high-resolution spectra from 425 nm to 700 nm.

2.4. Ab initio calculations

To perform our ab initio calculations, we have used spin-polarized density functional theory [34,35] and the projector augmented wave method (PAW) [36] as implemented in the VASP code [37,38]. In the PAW method, the Kohn-Sham wave function is expanded using a plane-wave basis that is augmented near the atoms in order to recover the full all-electron wave function. The exchange-correlation potential of Heyd, Scuseria, and Ernzerhof (HSE06) [39-41] was chosen because it has been shown to give reliable results for f-electrons systems [42]. Here the exchange part of the potential contains a part of Hartree-Fock exchange for the short-range part of the interaction, while the correlation potential is described by the generalized gradient approximation. The HSE06 functional is known to solve partly the problem of self-interaction and to provide band gaps in reasonable agreement with the experimental values. The geometry used in the calculations was that of the experimental structure obtained at 100 K. Although the calculations are performed at 0 K, the effect of using a structure obtained at a finite temperature will not have a significant effect on the electronic structure properties. The default cut-off for the

wave function and a *k*-point mesh of 2 × 2 × 2 to sample the Brillouin zone were used. Different magnetic states were checked, and it was found that an antiferromagnetic order of the magnetic moments on the U atoms gave the lowest total energy.

2.5. Resistivity measurements

Two-probe resistivity data were collected between 293 K and 500 K on a single crystal of $Ba_9Ag_{10}U_4S_{24}$ using a home-made resistivity apparatus equipped with a Keithley 617 electrometer and a high-temperature vacuum chamber controlled by a K-20 MMR system. Data acquisition was controlled by custom-written software. Graphite paint (PELCO isopropanol-based graphite paint) was used for electrical contacts with Cu wire of 0.025 mm thickness (Omega). Direct current was applied along an arbitrary direction.

3. Results

3.1. Synthesis

Single crystals of $Ba_9Ag_{10}U_4S_{24}$ were obtained in a high yield (□90%) at 1273 K by direct combination of U, BaS, Ag, and S. The XRPD pattern of the product was in good agreement with that calculated from the single-crystal structure but revealed minor contamination by UOS. The two materials could not be separated to afford a pure sample of $Ba_9Ag_{10}U_4S_{24}$. Thus, no meaningful magnetic data could be collected.

3.2 Multiphoton luminescence spectroscopy.

The luminescence spectrum of the sample of $Ba_9Ag_{10}U_4S_{24}$ is shown in Fig. 1. Strong broadband luminescence occurs because of multiphoton absorption of the excitation laser. Most of the luminescence lies at wavelengths beyond 532 nm, indicating that multiphoton absorption is dominated by two-photon absorption. The origin of the two photon absorption is a large second-order susceptibility, which can only occur in noncentrosymmetric materials. No second harmonic generation line is apparent in the spectrum because the sample is strongly absorbing at

532 nm. The presence of some luminescence at wavelengths shorter than 532 nm indicates that a weaker, cascaded three-photon absorption process was also present. Numerous emission lines are present, such as the one at 553 nm.

3.3. Structure

Given the above spectroscopic results the compound $Ba_9Ag_{10}U_4S_{24}$ must have a noncentrosymmetric structure. It crystallizes in a new structure type in the noncentrosymmetric space group C_{4v}^{10}–*I*4*cm* of the tetragonal system with four formula units in a cell with lattice constants a = 13.9189(6) Å and c= 23.7641(11) Å (volume = 4604.0(5) Å^3). Metrical data are reported in the Table 2. The asymmetric unit contains three Ba, five Ag, three U, and 10 S sites. The site symmetries are 4.. (Ba3, U3, S9, S10); 2.mm (U2, Ag4, Ag5); ..m (U1, Ag2, Ag3, S4, S5, S6, S7, S8); and 1 (Ba1, Ba2, Ag1, S1, S2, S3).

A general view of the structure down the *a* axis is showed in Fig. 2. All U atoms are octahedrally coordinated by S atoms; all Ag atoms are coordinated to four S atoms, except atom Ag3 which is surrounded by three S atoms. The network of these polyhedra, particularly the coordination of the Ag3 and Ag5 sites, is shown in Fig. 3. Each U1 atom is coordinated to two S1, two S3, one S5, and one S8 atom. The U1 octahedron shares four edges with the neighboring Ag1 polyhedron, one edge with the Ag3 polyhedron, and corners with Ag4 and Ag5 polyhedra. The local environment of atom U1 is viewed in Fig. 4. Each U2 atom is octahedrally coordinated to two S4, two S6, and two S7 atoms. Each U2 octahedron shares two edges with Ag2 tetrahedra, one edge with an Ag4 polyhedron, one edge with an Ag5 polyhedron, and two corners with an Ag3 polyhedron. These polyhedra are displayed in Fig. 5 as well. The U3 atom is octahedrally coordinated by four S2, one S9, and one S10 atom. This octahedron shares four S2 corners with Ag2 polyhedra. Fig. 6 presents the local coordination of atom U3.

The Ag1, Ag2, and Ag4 atoms are tetrahedrally coordinated by four S atoms; the Ag3 atom is surrounded by three S atoms in a triangular fashion; finally, the Ag5 atom is located in a slightly distorted seesaw formed by two S5 and two S6 atoms.

The overall structure consists of a complex three-dimensional stacking of U and S polyhedra. The Ba1 and Ba2 atoms occupy linearly the resultant channels, whereas the Ba3 atoms are positioned in the centers of cages formed by the U1 octahedra and $AgnS_4$ (n=1,2,4, and 5) polyhedra.

The stabilization of the C_{4v}^{10}–*I*4*cm* noncentrosymmetric structure rather than the centrosymmetric D_{4h}^{18}–*I*4/*mcm* structure is caused by the presence of the $Ag3S_3$ polyhedra on the top of the U1 atoms (Fig. 4). This steric effect results in the slight shift of the U1 atoms down the *c* axis at $z = 0.24592(3)$ rather than 0.25 and leads to the polar non-centrosymmetric structure.

3.4. Electronic properties

Using the HSE functional, we have computed the electronic structure of $Ba_9Ag_{10}U_4S_{24}$. The total and partial density of states (PDOS) are presented in Fig. 7. The total density of states is not polarized in spin because $Ba_9Ag_{10}U_4S_{24}$ is found to be antiferromagnetic. The electronic band gap is found to be 2.1 eV. Note that the HSE functional generally gives reliable values for band gaps [42]. For the U atoms, the PDOS corresponding to three inequivalent atoms are plotted, whereas for S, Ba, and Ag only one PDOS is presented because the differences among plots of the same element remain small. The spin polarization of the U atoms is seen clearly on the corresponding PDOS plots, and induces a small magnetic moment on the S atoms, but not on the Ba or Ag atoms. In particular, the magnetic moments on the U1 atoms are arranged antiferromagnetically with respect to the U2 and U3 magnetic moments. The f states contribute up to the Fermi level. Moreover, the inequivalence of the U atoms is seen from the position of the f electron level. These are around −1.5 eV, −1 eV, and −1.2 eV for U1, U2, and U3, respectively. Also, we observe that the maximum of the valence band corresponds to S and Ba states, whereas the minimum of the conduction band corresponds to U-f states.

3.5. Resistivity

High temperature-dependent resistivity data on a single crystal of $Ba_9Ag_{10}U_4S_{24}$ along an arbitrary direction show semiconducting behavior. The resistivity decreases from 178 Ohm.cm at 293 K to 75 Ohm.cm at 500 K. That the Arrhenius plot (Fig. 8) of the resistivity data is non-

linear suggests a complex activation mechanism with activation energies ranging from 0.03(1) eV to 0.08(1) eV. $Ba_9Ag_{10}U_4S_{24}$ is much less resistive than the quaternary compounds Ba_3FeUS_6 (1.4 kOhm.cm at 300 K) and Ba_3AgUS_6 (5.5 MOhm.cm at 300 K) [17]. The activation energy of $Ba_9Ag_{10}U_4S_{24}$ is also smaller than the value of 0.12 eV estimated for Ba_3FeUS_6

3.6. Formal oxidation states

In the $Ba_9Ag_{10}U_4S_{24}$ structure each U atom is octahedrally coordinated by six S atoms. The ranges of U−S distances are: U1, 2.560(3) Å−2.753(5) Å; U2, 2.596(4) Å–2.624(4) Å; U3, 2.538(5) Å–2.613(2) Å. These distances are short compared with typical U^{4+}−S distances but compare favorably with the U^{5+}−S distances in $K_2Cu_3US_5$ [16] (2.587(1)Å−2.682(1)Å) and Ba_3AgUS_6 (2.609(1) Å). Other examples may be found in Table 3. Except for $Rb_4U_4P_4Se_{26}$ [14], all the other pentavalent chalcogenides possess U in octahedral coordination. The Ag–S distances in the $Ba_9Ag_{10}U_4S_{24}$ structure are typical for Ag^{1+}−S. For the Ag1, Ag2, Ag4, and Ag5 atoms, which are each coordinated to four S atoms, the Ag–S distances range from 2.526(2) Å to 2.852(4) Å. These distances are in agreement with those found in compounds in which Ag is four coordinate, for example Ag_2CdGdS_4 [43], 2.522 Å–2.570 Å; $BaAg_2S_2$ [44], 2.659(5) Å–2.686(2) Å; $CsAgSb_4S_7$ [45], 2.502(1) Å–2.864(1) Å; $KAg(SCN)_2$ [46],2.577(6) Å–2.7262(5) Å; and $La_4Ag_2In_4S_{13}$ [47], 2.659(1) Å– 2.933(1) Å. The Ag3 atoms are coordinated to three S atoms with shorter distances of 2.358(4) Å and 2.429(3) Å and may be compared with those found in compounds in which Ag is three-coordinate, for example $AgGePr_3S_7$ (2.356 Å) and $AgNd_3SiS_7$ (2.372 Å) [48]. The Ba–S distances in the $Ba_9Ag_{10}U_4S_{24}$ structure range between 3.095(3) Å and 3.461(6) Å and are typical of those encountered in $BaUS_3$, BaU_2S_5, $Ba_{3.69}US_6$ [22], Ba_2US_6 [42], and $Ba_2Cu_2AnS_5$ (An = Th, U) [27,28].

The assignment of formal oxidation states in $Ba_9Ag_{10}U_4S_{24}$ may be made as follows: From the comparisons above the compound contains Ba^{2+} and Ag^{1+}. There are no short S–S interactions in the structure and hence no S_2^{2-} species. Then with charge balance in mind there are three possibilities for the U oxidation state, namely (i) 2 U^{4+}+2 U^{6+}; (ii) 1 U^{4+} + 1 U^{6+} + 2 U^{5+}; or (iii) 4 U^{5+}. We favor possibility (iii), namely that $Ba_9Ag_{10}U_4S_{24}$ is another example of a U^{5+} compound, for the following reasons: (1) the differences among U1−S, U2−S, and U3−S

distances in the structure are small and (2) they are generally shorter than those in typical $U^{4+,5+}$ compounds (Table 3). Moreover, although strictly empirical it is interesting that Bond Valence Sum analysis [49] as implemented in PLATON [31] provided the following valences for $Ba_9Ag_{10}U_4S_{24}$: U1, 4.667; U2, 5.095; U3, 5.434; Ba1, 2.413; Ba2, 2.267; Ba3, 1.804; Ag1, 1.146; Ag2, 1.213; Ag3, 1.388; Ag4, 0.904; and Ag5, 0.926.

3.7. Stabilization of U^{5+} Chalcogenides

Significant progress has been made in stabilizing U^{5+} through the use of reliable pathways such us reducing UO_2^{2+} to UO_2^{1+}, or oxidizing U^{3+} or U^{4+} to U^{5+}. [1] These techniques apply to molecular or organoactinide compounds and require the use of wet chemical methods. Moreover, some U^{5+}oxides have been stabilized by the reduction of the U^{6+} under a flow of Ar-H_2(5%) [5,6]. Conversely, exploratory synthesis by its very nature most often leads to reaction products that could not be predicted in advance. Thus, U^{5+} chalcogenides are rare and most were obtained serendipitously. However, with the increase in the number of the U^{5+} chalcogenide examples [14-17,22-24], some observations can be made. The use of halides precursors may favor the formation of pentavalent uranium chalcogenides [15]. Conceptually, substitution of cations of different charges into a structure type may be useful. Consider compounds crystallizing in the K_4CdCl_6 structure type [50]. The compound $Ba_{3.69}U^{4+,5+}S_6$ [22] was synthesized in an exploration of possible Ba/U/V/S quaternaries. The flexibility of this structure type allowed the synthesis of two other compounds by insertion of Fe^{2+} and Ag^{+} to form Ba_3FeUS_6 and Ba_3AgUS_6. These contain U^{4+} and U^{5+}, respectively [17]. Another flexible structure is that of $Ba_7M_2US_{12.5}O_{0.5}$ [51] with M = V, Fe. When V^{4+} was replaced by Fe^{3+} in an attempt to change the oxidation state of U from +4 to +5 S−S bonds were created via the formation of Fe_2S_8 species to keep U in its oxidation state +4. Apparently, energetically the formation of an S−S bond was favored over the oxidation of U^{4+} to U^{5+}. In the present instance the compound $Ba_9Ag_{10}U_4S_{24}$ resulted from an attempt to synthesize the Ag analogue of $Ba_2Cu_2US_5$ [27]. General pathways for the stabilization of U^{5+} in solid-state chalcogenides remain elusive.

4. Conclusions

A noncentrosymmetric uranium sulfide, namely $Ba_9Ag_{10}U_4S_{24}$, was synthesized by direct combination of BaS, Ag, U, and S at 1273 K. This compound crystallizes in a new structure type in space group C_{4v}^{10}–$I4cm$ of the tetragonal system. DFT calculations predict an antiferromagnetic ground state and a band gap of 2.1 eV. Resistivity measurements indicate that the compound is a semiconductor with a complex activation mechanism and activation energies ranging from 0.03(1) eV to 0.08(1) eV. The U−S distances are typical of those in known U^{5+} sulfides. The overall structure charge balances with 9 Ba^{2+}, 10 Ag^{1+}, 4 U^{5+} and 24 S^{2-}. Thus $Ba_9Ag_{10}U_4S_{24}$ is another example of a relatively rare U^{5+} compound among the family of uranium chalcogenides.

Acknowledgments

This research was kindly supported at Northwestern University by the U.S. Department of Energy, Basic Energy Sciences, Chemical Sciences, Biosciences, and Geosciences Division and Division of Materials Science and Engineering Grant ER-15522. Use was made of the IMSERC X-ray Facility at Northwestern University, supported by the International Institute of Nanotechnology (IIN). S. L. acknowledges HPC resources from GENCI-CCRT/CINES (Grant x2014-085106). N. L. F. acknowledges Grant NSF IGERT DGE-0801685.

References

[1] C.R. Graves, J.L. Kiplinger, Chem. Commun. 2009 (2009) 3831-3853.

[2] J.T. Stritzinger, E.V. Alekseev, M.J. Polinski, J.N. Cross, T.M. Eaton, T.E. Albrecht-Schmitt, Inorg. Chem. doi.org/10.1021/ic500523a (2014) .

[3] N. Belai, M. Frisch, E.S. Ilton, B. Ravel, C.L. Cahill, Inorg. Chem. 47 (2008) 10135-10140.

[4] E.S. Ilton, A. Haiduc, C.L. Cahill, A.R. Felmy, Inorg. Chem. 44 (2005) 2986-2988.

[5] S. Van den Berghe, A. Leenaers, C. Ritter, J. Solid State Chem. 177 (2004) 2231-2236.

[6] A.V. Soldatov, D. Lamoen, M.J. Konstantinovic, S. Van den Berghe, A.C. Scheinost, M. Verwerft, J. Solid State Chem. 180 (2007) 54-61.

[7] D.E. Bugaris, J.A. Ibers, Dalton Trans. 39 (2010) 5949-5964.

[8] A.A. Narducci, J.A. Ibers, Chem. Mater. 10 (1998) 2811-2823.

[9] E. Manos, M.G. Kanatzidis, J.A. Ibers, Actinide Chalcogenide Compounds, in: L.R. Morss, N.M. Edelstein, J. Fuger (Eds.), The Chemistry of the Actinide and Transactinide Elements, 4th ed., Vol. 6, Springer, Dordrecht, The Netherlands, 2010, p. 4005-4078.

[10] S.A. Sunshine, D. Kang, J.A. Ibers, J. Am. Chem. Soc. 109 (1987) 6202-6204.

[11] W.H. Zachariasen, Acta Cryst. 2 (1949) 291-296.

[12] A. Daoudi, H. Noël, J. Less-Common Met. 115 (1986) 253-259.

[13] R. Julien, N. Rodier, V. Tien, Acta Crystallogr. Sect. B: Struct. Crystallogr. Cryst. Chem. 34 (1978) 2612-2614.

[14] K. Chondroudis, M.G. Kanatzidis, J. Am. Chem. Soc. 119 (1997) 2574-2575.

[15] D.E. Bugaris, E.S. Choi, R. Copping, P.-A. Glans, S.G. Minasian, T. Tyliszczak, S.A. Kozimor, D.K. Shuh, J.A. Ibers, Inorg. Chem. 50 (2011) 6656-6666.

[16] D.L. Gray, L.A. Backus, H.-A. Krug von Nidda, S. Skanthakumar, A. Loidl, L. Soderholm, J.A. Ibers, Inorg. Chem. 46 (2007) 6992-6996.

[17] A. Mesbah, C.D. Malliakas, S. Lebègue, A.A. Sarjeant, W. Stojko, L.A. Koscielski, J.A. Ibers, Inorg. Chem. 53 (2014) 2899-2903.

[18] M.D. Ward, A. Mesbah, S.G. Minasian, D.K. Shuh, T. Tyliszczak, M. Lee, E.S. Choi, S. Lebègue, J.A. Ibers, Inorg. Chem. 53 (2014) 6920-6927.

[19] T. Vovan, N. Rodier, C. R. Seances Acad. Sci., Ser. C 289 (1979) 17-20.

[20] T. Fujino, N. Sato, K. Yamada, H. Masuda, M. Wakeshima, J. Alloys Compd. 271-273 (1998) 452-455.

[21] A. Daoudi, H. Noël, Inorg. Chim. Acta 117 (1986) 183-185.

[22] A. Mesbah, J.A. Ibers, J. Solid State Chem. 199 (2013) 253-257.

[23] D.E. Bugaris, J.A. Ibers, Inorg. Chem. 51 (2012) 661-666.

[24] C.D. Malliakas, J. Yao, D.M. Wells, G.B. Jin, S. Skanthakumar, E.S. Choi, M. Balasubramanian, L. Soderholm, D.E. Ellis, M.G. Kanatzidis, J.A. Ibers, Inorg. Chem. 51 (2012) 6153-6163.

[25] D.E. Bugaris, J.A. Ibers, J. Solid State Chem. 181 (2008) 3189-3193.

[26] A.J.K. Haneveld, F. Jellinek, J. Less-Common Met. 18 (1969) 123-129.

[27] H.-yi Zeng, J. Yao, J.A. Ibers, J. Solid State Chem. 181 (2008) 552-555.

[28] A. Mesbah, Lebegue.S, J.M. Klingsporn, W. Stojko, R.P. Van Duyne, J.A. Ibers, J. Solid State Chem. 200 (2013) 349-353.

[29] Bruker APEX2 Version 2009.5-1 Data Collection and Processing Software,, Bruker Analytical X-Ray Instruments, Inc., Madison, WI, USA, 2009.

[30] G.M. Sheldrick, SADABS, 2008. Department of Structural Chemistry, University of Göttingen, Göttingen, Germany

[31] A.L. Spek, PLATON, A Multipurpose Crystallographic Tool, 2014. Utrecht University, Utrecht, The Netherlands

[32] G.M. Sheldrick, Acta Crystallogr. Sect. A: Found. Crystallogr. 64 (2008) 112-122.

[33] L.M. Gelato, E. Parthé, J. Appl. Crystallogr. 20 (1987) 139-143.

[34] P. Hohenberg, W. Kohn, Phys. Rev. 136 (1964) 864-871.

[35] W. Kohn, L.J. Sham, Phys. Rev. 140 (1965) 1133-1138.

[36] P.E. Blöchl, Phys. Rev. B 50 (1994) 17953-17979.

[37] G. Kresse, J. Forthmüller, Comput. Mater. Sci. 6 (1996) 15-50.

[38] G. Kresse, D. Joubert, Phys. Rev. B 59 (1999) 1758-1775.

[39] J. Heyd, G.E. Scuseria, M. Ernzerhof, J. Phys. Chem. 118 (2003) 8207-8215.

[40] J. Paier, M. Marsman, K. Hummer, G. Kresse, I.C. Gerber, J.G. Angyan, J. Chem. Phys. 125 (2006) 249901-1-2.

[41] J. Heyd, G.E. Scuseria, M. Ernzerhot, J. Chem. Phys. 124 (2006) 219906-1.

[42] A. Mesbah, E. Ringe, S. Lebègue, R.P. Van Duyne, J.A. Ibers, Inorg. Chem. 51 (2012) 13390-13395.

[43] O.V. Parasyuk, L.V. Piskach, I.D. Olekseyuk, V.I. Pekhnyo, J. Alloys Compd. 397 (2005) 95-98.

[44] W. Bronger, B. Lenders, J. Huster, Z. Anorg. Allg. Chem. 623 (1997) 1357-1360.

[45] F.Q. Huang, J.A. Ibers, J. Solid State Chem. 178 (2005) 212-217.

[46] H. Krautscheid, S. Gerber, Acta Crystallogr. Sect. C: Cryst. Struct. Commun. C57 (2001) 781-783.

[47] L.D. Gulay, M. Daszkiewicz, M.R. Huch, J. Solid State Chem. 181 (2008) 2626-2632.

[48] M. Guittard, M. Julien-Pouzol, Bull. Soc. Chim. Fr. (1970) 2467-2469.

[49] I.D. Brown, The Chemical Bond in Inorganic Chemistry, The Bond Valence Model, Oxford University Press, New York, 2002.

[50] H.P. Beck, W. Milius, Z. Anorg. Allg. Chem. 539 (1986) 7-17.

[51] A. Mesbah, W. Stojko, C.D. Malliakas, S. Lebegue, N. Clavier, J.A. Ibers, Inorg. Chem. 52 (2013) 12057-12063.

Table 1

Crystal data and structure refinement for $Ba_9Ag_{10}U_4S_{24}$

	$Ba_9Ag_{10}U_4S_{24}$
fw (g mol^{-1})	4036.47
a (Å)	13.9189(6)
c (Å)	23.7641(11)
V (Å^3)	4604.0(5)
T (K)	100(2)
Z	4
Space Group	C_{4v}^{10}–$I4cm$
ρ (g cm^{-3})	5.823
μ (mm^{-1})	26.796
$R(F)$[a]	0.0227
$R_w(F_o^2)$[b]	0.0447

[a] $R(F) = \Sigma \big|\, |F_o| - |F_c| \,\big| \,/\, \Sigma |F_o|$ for $F_o^2 > 2\sigma(F_o^2)$.

[b] $R_w(F_o^2) = \{\Sigma\, w(F_o^2 - F_c^2)^2] \,/\, \Sigma w F_o^4\}^{1/2}$. For $F_o^2 < 0$, $w^{-1} = \sigma^2(F_o^2)$; for $F_o^2 \geq 0$, $w^{-1} = \sigma^2(F_o^2) + (0.001F_o^2)^2$

Table 2

Selected interatomic distances in $Ba_9Ag_{10}U_4S_{24}$

atom–atom	distance (Å)	atom–atom	distance (Å)
U1–S1	2.662(3) × 2	Ag1–S1	2.674(3)
U1–S3	2.560(3) × 2	Ag1–S3	2.593(3)
U1–S5	2.753(5)	Ag1–S5	2.543(3)
U1–S8	2.700(5)	Ag1–S8	2.532(3)
U2–S4	2.596(4) × 2	Ag2–S2	2.526(2) × 2
U2–S6	2.624(4) × 2	Ag2–S4	2.585(5)
U2–S7	2.612(3) × 2	Ag2–S6	2.611(4)
U3–S2	2.613(2) × 4	Ag3–S1	2.429(3) × 2
U3–S9	2.538(5)	Ag3–S6	2.358(4)
U3–S10	2.539(6)	Ag4–S8	2.738(4) × 2
		Ag4–S4	2.612(5) × 2
U1•••Ag3	3.159(2)	Ag5–S5	2.534(4) × 2
		Ag5–S6	2.852(5) × 2

Table 3

U–S interatomic distances and oxidation states in selected uranium sulfides

compound	U oxidation state	U–S range (Å)[a]	reference
$BaUS_3$	4	2.698(1)–2.696(1)	[22]
Ba_3FeUS_6	4	2.715(1)	[17]
$Ba_8Hg_3U_3S_{18}$	mixed +4/+5	2.571(4)–2.743(3)	[23]
		2.595(4)–2.758(3)	
		2.602(4)–2.745(3)	
$Ba_{3.69}US_6$	mixed +4/+5	2.658(1)	[22]
$Ba_9Ag_{10}U_4S_{24}$	5	2.560(3)–2.753(5) (U1)	This work
		2.596(4)–2.624(4) (U2)	This work
		2.538(5)–2.613(2) (U3)	This work
Ba_3AgUS_6	5	2.609(1)	[17]
$K_2Cu_3US_5$	5	2.587(1)–2.683(1)	[16]
$Cs_6Cu_{12}U_2S_{15}$	mixed +5/+6	2.598(2)	[24]

[a]To facilitate comparisons in this table distances from the original cif files have been rounded where necessary to three significant figures.

Figure Captions

Fig. 1. Multiphoton fluorescence spectrum for $Ba_9Ag_{10}U_4S_{24}$ (1064 nm excitation).

Fig. 2. General view approximately down the *a* axis of the $Ba_9Ag_{10}U_4S_{24}$ structure.

Fig. 3. The US_6, AgS_4, and AgS_3 networks in the $Ba_9Ag_{10}U_4S_{24}$ structure.

Fig. 4. Local coordination of atom U1 in the $Ba_9Ag_{10}U_4S_{24}$ structure .

Fig. 5. Local coordination of atom U2 in the $Ba_9Ag_{10}U_4S_{24}$ structure.

Fig. 6. Local coordination of atom U3 in the $Ba_9Ag_{10}U_4S_{24}$ structure.

Fig. 7. Total (upper plot) and partial density of states (lower plots) of $Ba_9Ag_{10}U_4S_{24}$ For each atom, the PDOS is projected onto the relevant orbitals. The Fermi level is set at 0.

Fig. 8. Resistivity and the corresponding Arrhenius plots for $Ba_9Ag_{10}U_4S_{24}$.

figure 1

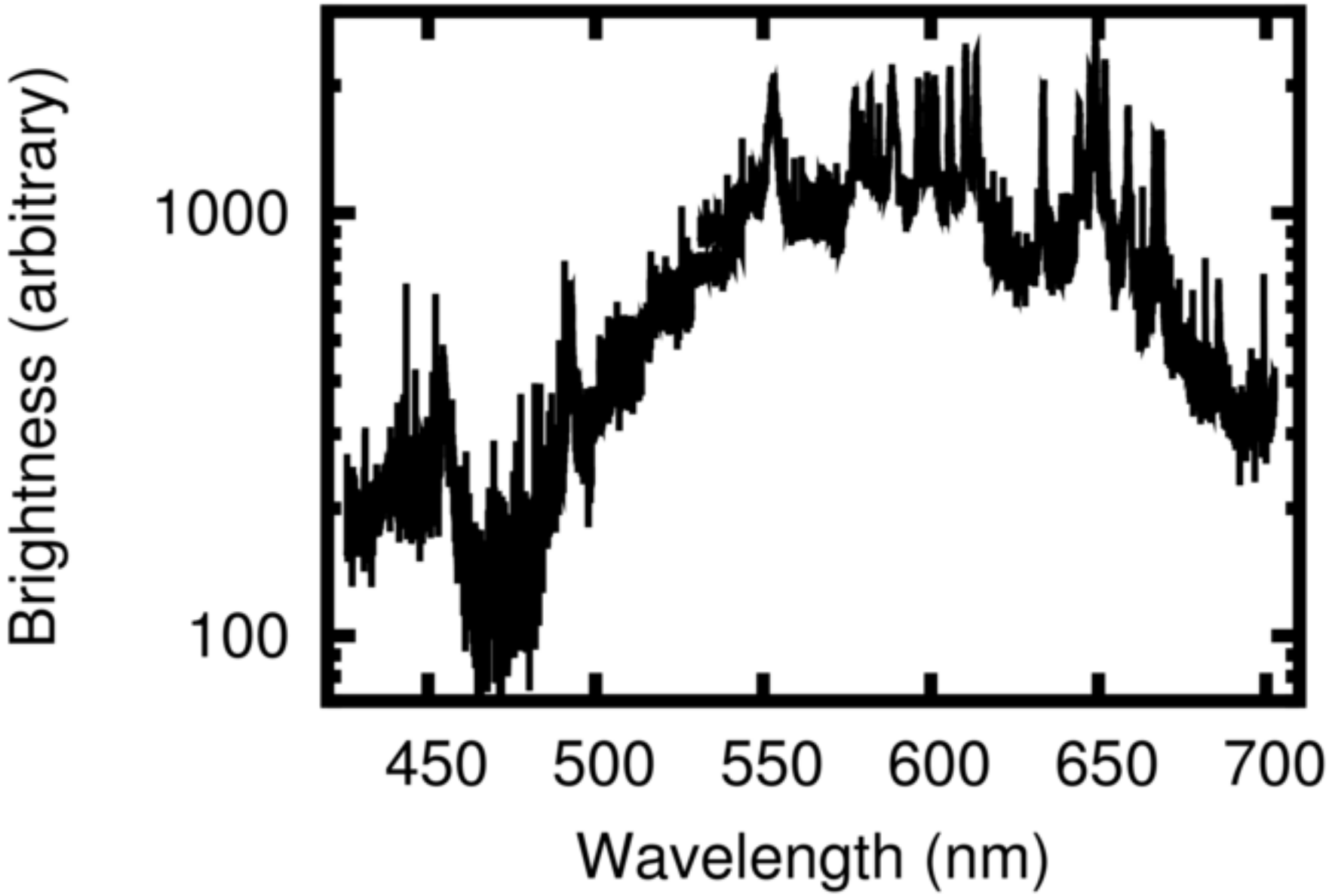
Brightness (arbitrary)
1000
100
450
500
550
600
650
700
Wavelength (nm)

figure 2

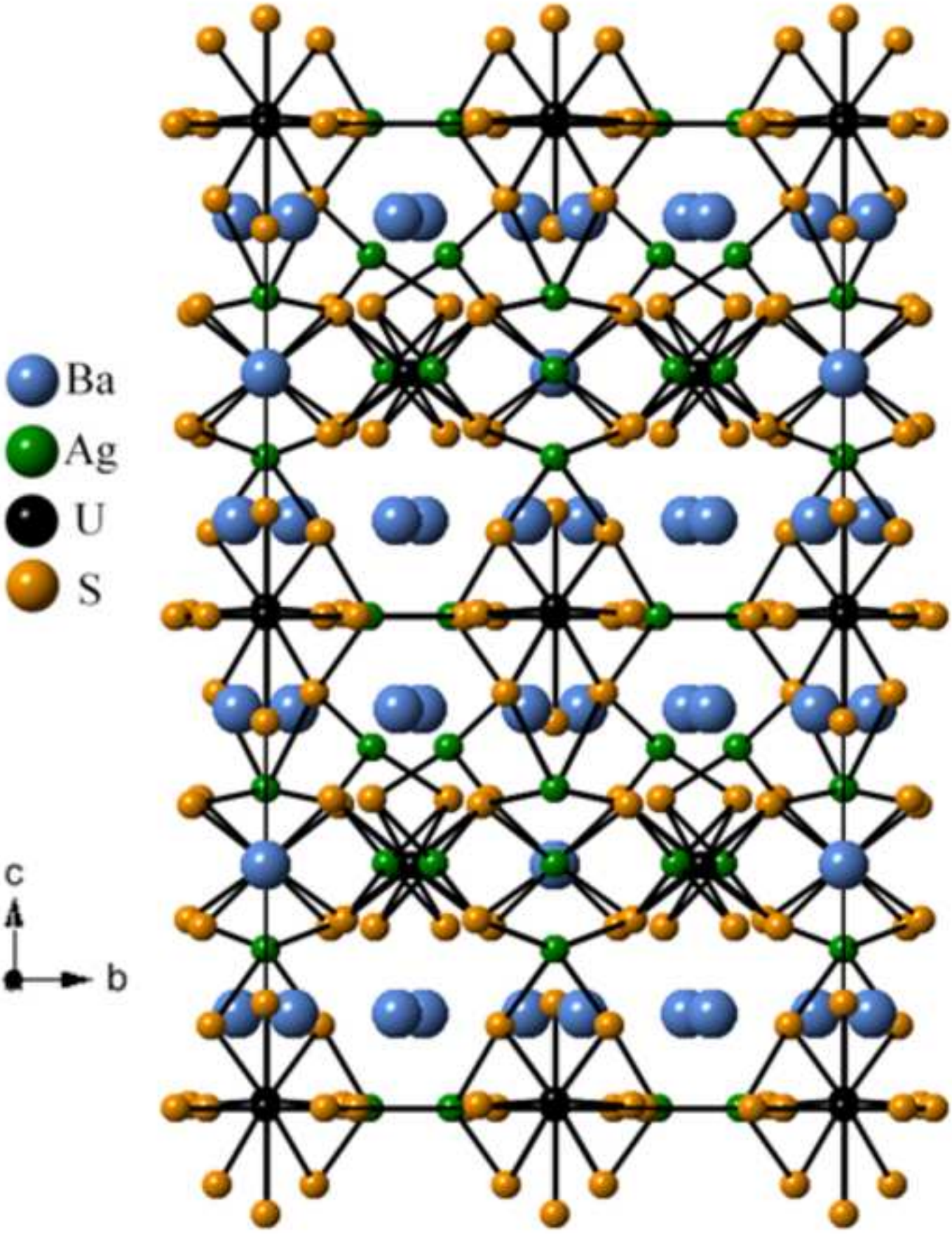

figure 3

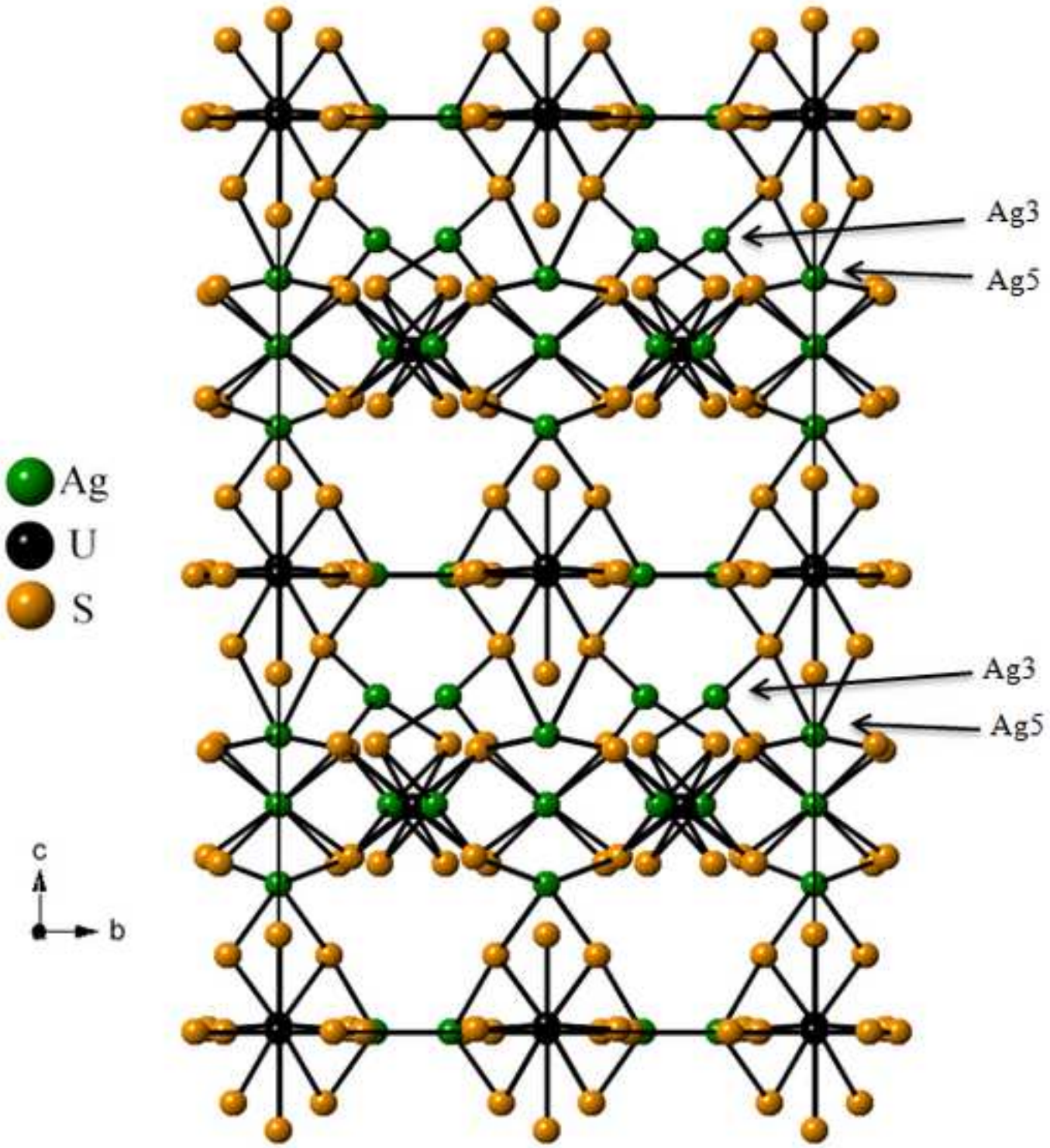

figure 4

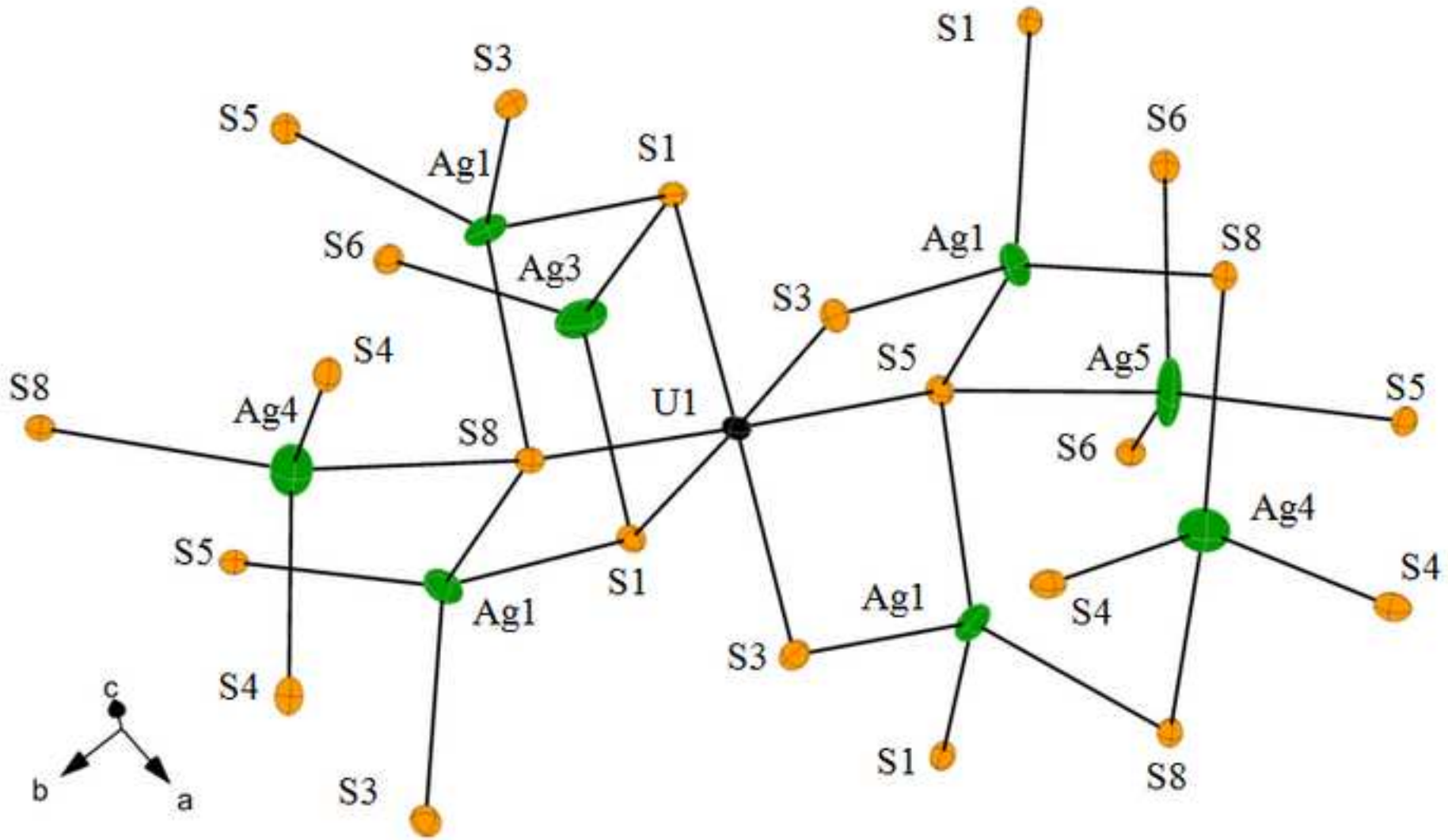
S1
S3
S5
Ag1
S1
S6
S6
Ag3
Ag1
S8
S3
S4
S5
Ag5
S8
Ag4
U1
S5
S8
S6
Ag4
S5
S1
S4
S4
Ag1
Ag1
S3
S4
S1
S8
S3
c
b
a

figure 5

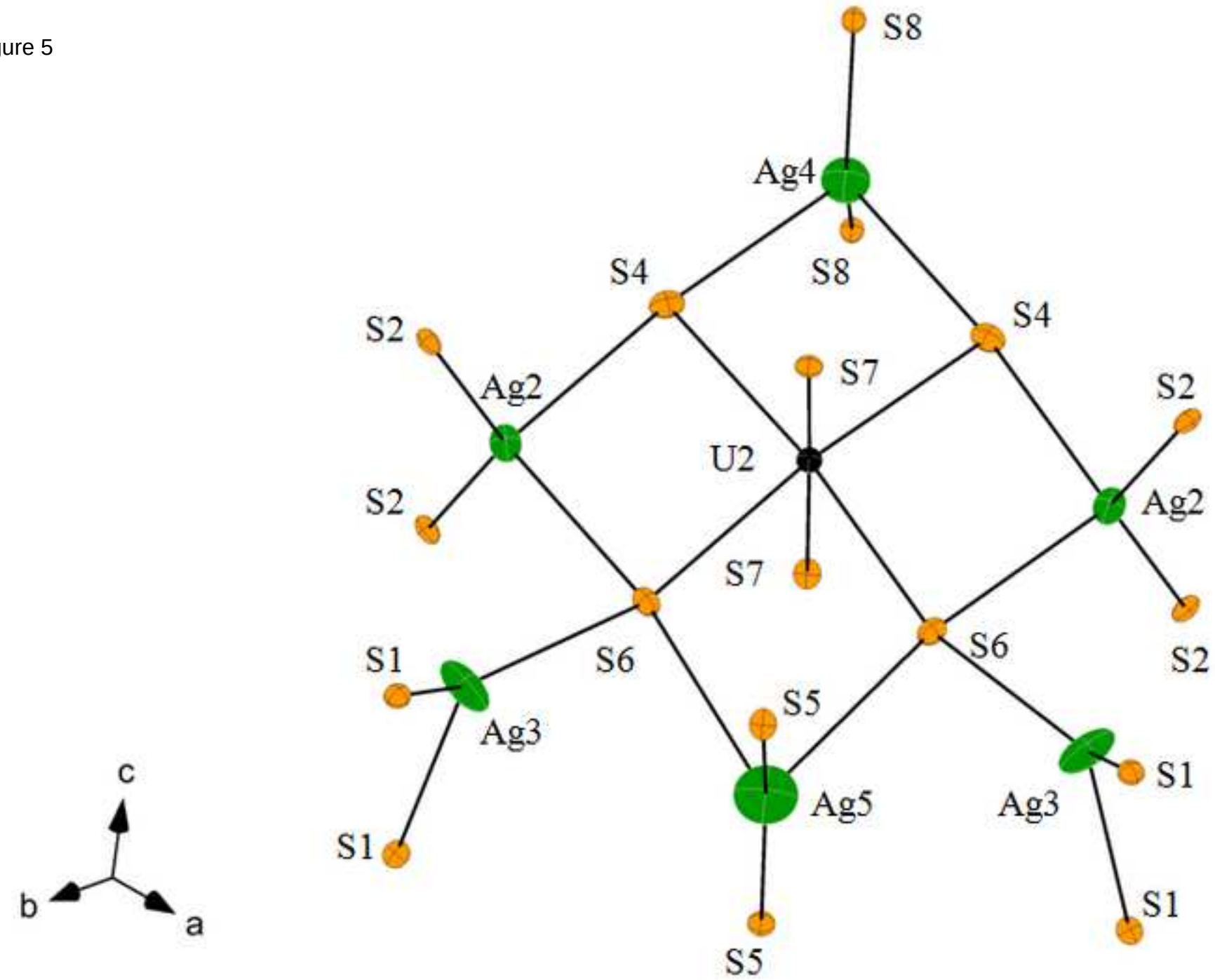
S8
Ag4
S8
S4
S4
S2
S7
S2
Ag2
U2
S2
Ag2
S7
S6
S6
S2
S1
S5
Ag3
Ag5
Ag3
S1
S1
S1
S5
c
b
a

figure 6

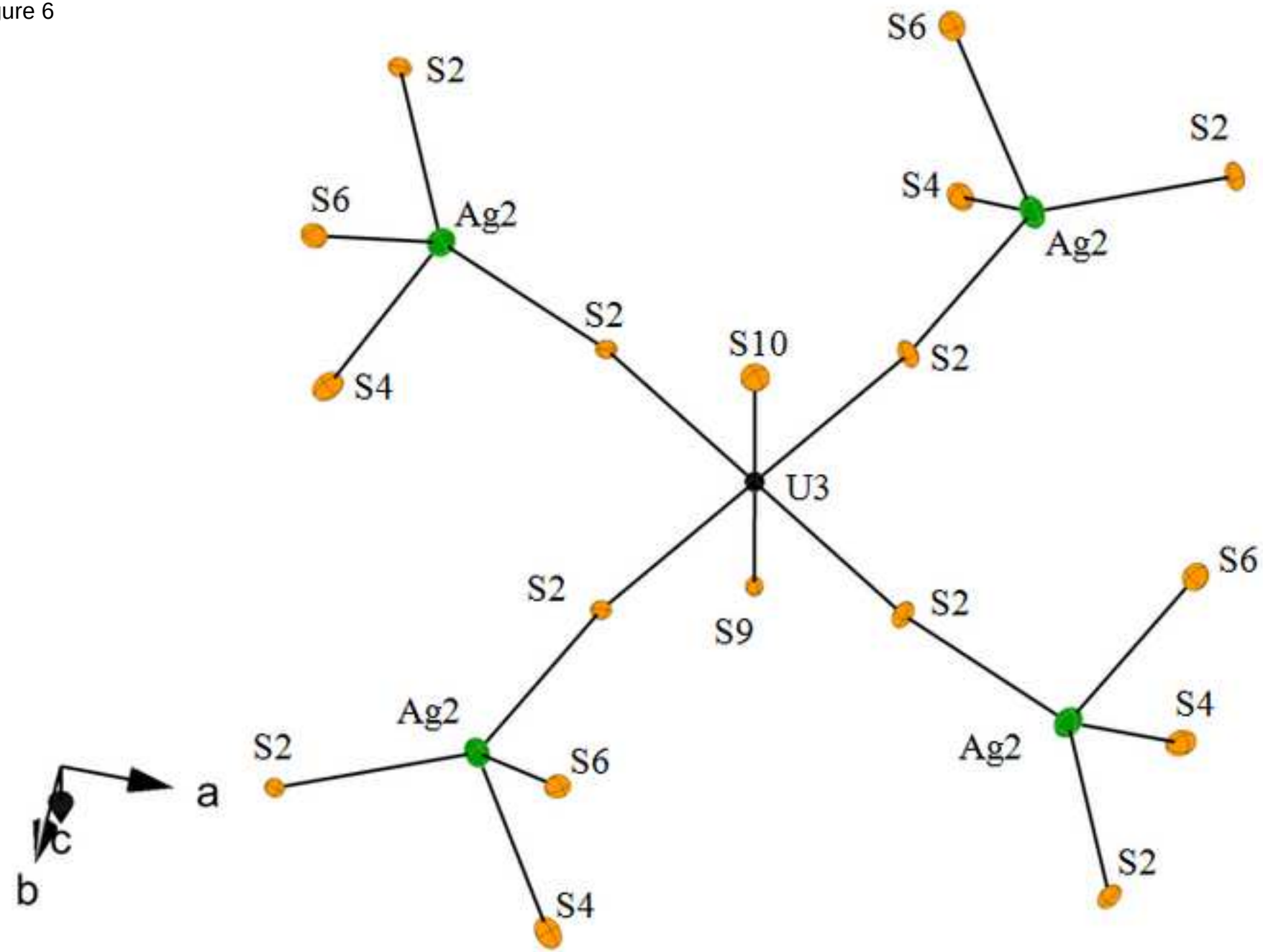
S6
S2
S2
S6
Ag2
S4
Ag2
S2
S10
S2
S4
U3
S2
S6
S2
S9
S2
Ag2
S4
S2
S6
Ag2
S4
S2
a
c
b

figure7

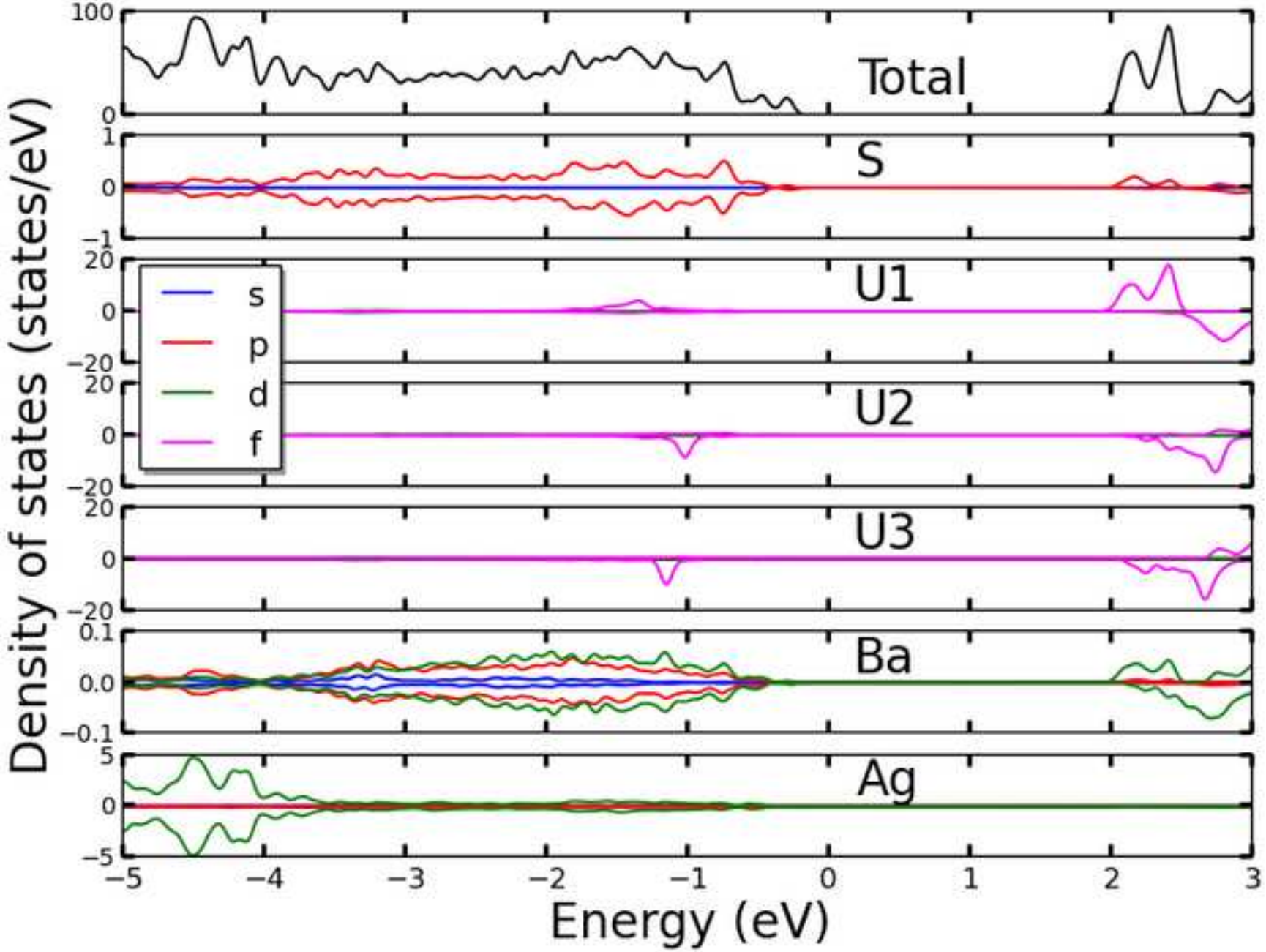
Total
S
U1
U2
U3
Ba
Ag
s
p
d
f
Density of states (states/eV)
Energy (eV)
100
0
1
0
−1
20
0
−20
20
0
−20
20
0
−20
0.1
0.0
−0.1
5
0
−5
−5
−4
−3
−2
−1
0
1
2
3

figure 8

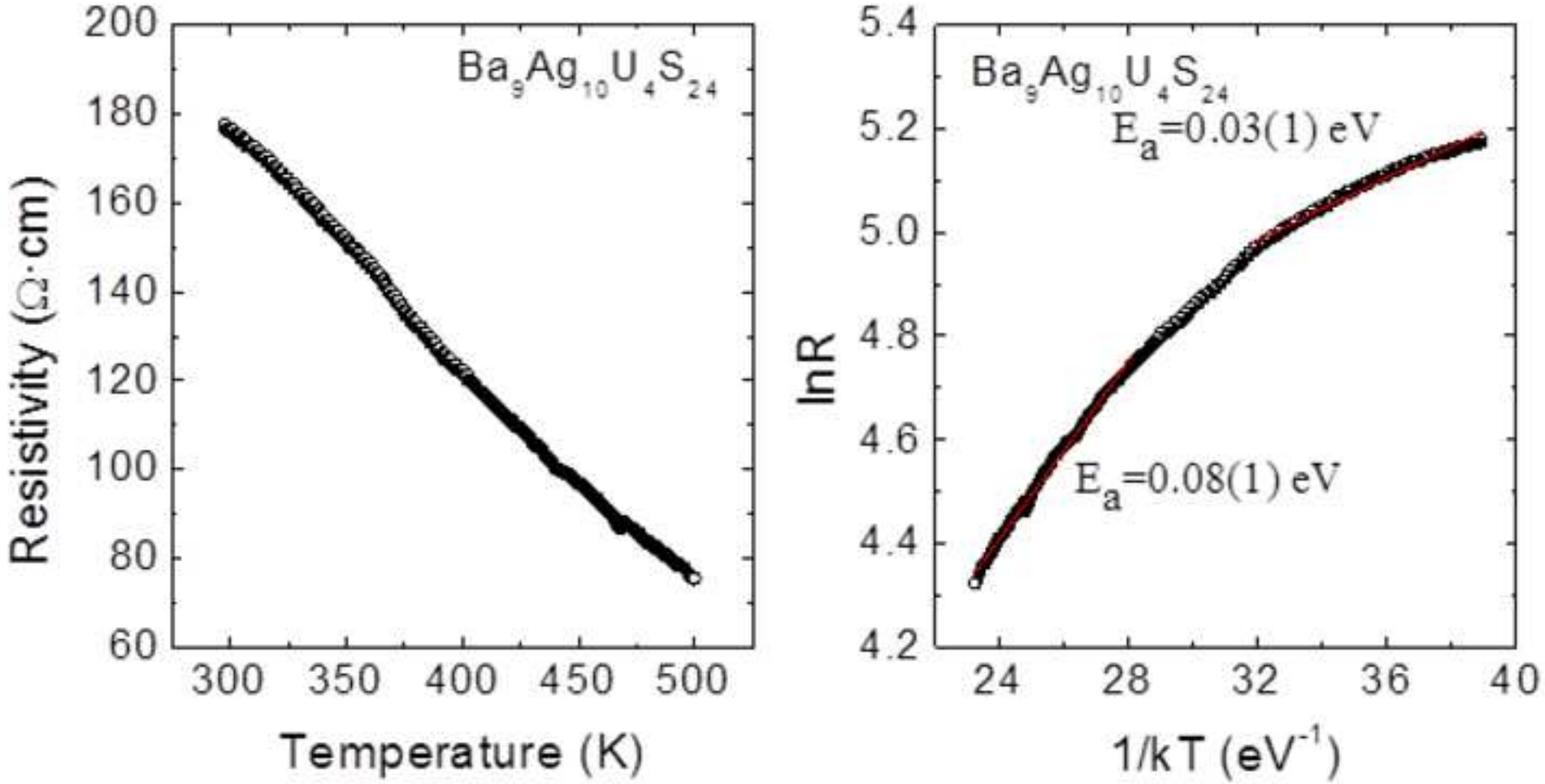
Ba9Ag10U4S24
Resistivity (Ω·cm)
Temperature (K)
200
180
160
140
120
100
80
60
300
350
400
450
500
Ba9Ag10U4S24
Ea=0.03(1) eV
Ea=0.08(1) eV
lnR
1/kT (eV-1)
5.4
5.2
5.0
4.8
4.6
4.4
4.2
24
28
32
36
40

*Graphical Abstract (TOC Figure)

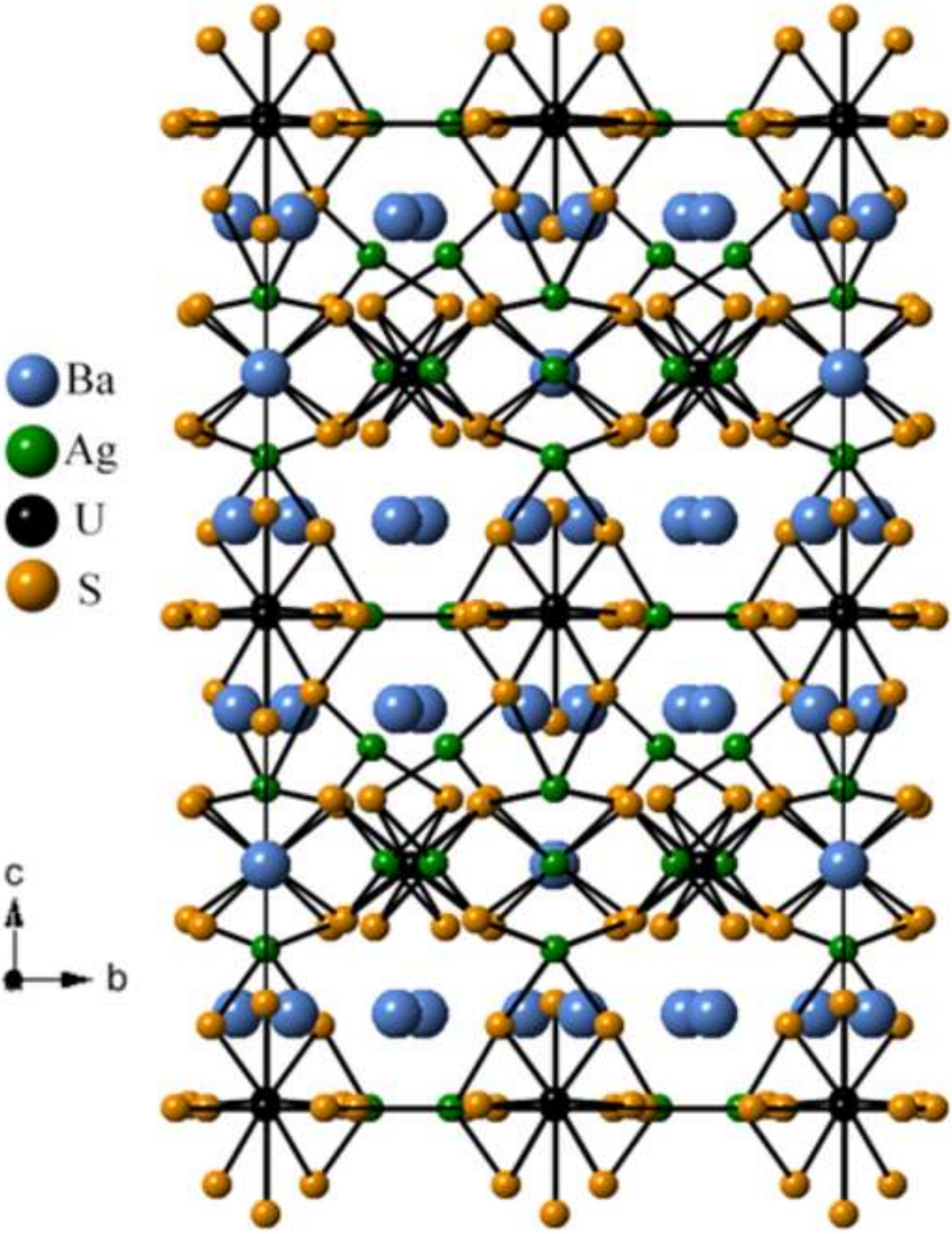

***Graphical Abstract Legend (TOC Figure)**

General view of the $Ba_9Ag_{10}U_4S_{24}$ structure.